

Conformational Flexibility of C8-Phenoxy-2'-deoxyguanosine Nucleotide Adducts

Andrea L. Millen,[†] Richard A. Manderville,[†] and Stacey D. Wetmore^{*,†}

Department of Chemistry, University of Lethbridge, 4401 University Drive, Lethbridge, Alberta, Canada, T1K 3M4, Department of Chemistry, University of Guelph, Guelph, Ontario, Canada, N1G 2W1

Received: December 18, 2009; Revised Manuscript Received: February 2, 2010

Previous computational work suggests that isolated C8-phenoxy-2'-deoxyguanosine nucleoside adducts preferentially adopt a *syn* orientation about the glycosidic bond, which is the first step in the mechanism by which many bulky C8 adducts exert their mutagenic effects. Since it is not clear whether these results can be directly extrapolated to the preferred conformation in DNA helices, approaches that more accurately reflect the physiological environment were used in the present study to understand the *anti/syn* preference of the *ortho* and *para* C8-phenoxy-2'-deoxyguanosine adducts. Using nucleoside models and methods (B3LYP) similar to those previously implemented, we determine that the *syn* conformer is less stable than previously predicted when geometries relevant to B-DNA are considered. This indicates that the conformational energy trend is model dependent and stresses the importance of considering models that better mimic the DNA environment when determining the conformational preference of damaged bases. Therefore, we expanded our computational model to include the 5'-monophosphate group. Since the correct *anti/syn* energy trend for 2'-deoxyguanosine (dG) 5'-monophosphate has only been found using very specific computational models and prior knowledge of the biologically relevant nucleotide conformation, which is unavailable for most damaged systems, we initially benchmark our computational approach by studying the natural nucleotide. Despite the wide use of gas-phase optimizations in the current literature, only through the implementation of solvation-phase optimizations, as well as the use of a counterion model for the phosphate backbone, is the correct *anti/syn* energy trend predicted. Indeed, this is the first time in the literature that a biologically relevant *syn* structure is characterized for dG using methods suitable for studying bulky DNA adducts. Subsequently, our newly identified approach for DNA lesions was used to study C8-phenoxy DNA adducts. In contrast to previously published results, we predict that the *ortho* and *para* adducts may adopt both the *anti* and *syn* conformations in DNA helices. These results have implications for the base-pairing properties and mutagenicity of these adducts, which must be further considered in future work.

Introduction

Nucleobase analogues can be designed to have many desirable properties,^{1–3} including enhanced fluorescence^{4,5} and flexibility.⁶ These modified bases are of interest for their potential use as bioprobes,^{7,8} inhibitors,⁹ or designer molecules for other applications in nanotechnology¹⁰ and biochemistry.¹¹ However, modified DNA can also appear in nature as a product of damaging (cellular) processes such as oxidation^{12–15} or alkylation.^{16–18} In addition, exogenous DNA damage can occur upon exposure to carcinogenic compounds found in the environment. This latter type of damage typically results in the formation of addition products (adducts), where the carcinogens or their metabolites covalently bind to DNA and generate bulky nucleobases.^{19–23} Unfortunately, if unrepaired, this damage can lead to mutagenic changes in DNA, and therefore detection of DNA modifications can serve as biomarkers for cancer and other diseases.^{24,25}

Our group has recently become interested in the properties of the bulky C8-aryl-2'-deoxyguanosine adducts formed upon exposure to aryl groups (see, for example, Figure 1).²⁶ Although a variety of C8-aryl adducts are known,^{19–23} we are particularly interested in those formed due to phenolic toxins.^{26–35} Upon metabolic activation, these compounds undergo transformation to an unstable phenoxy radical intermediate that can directly

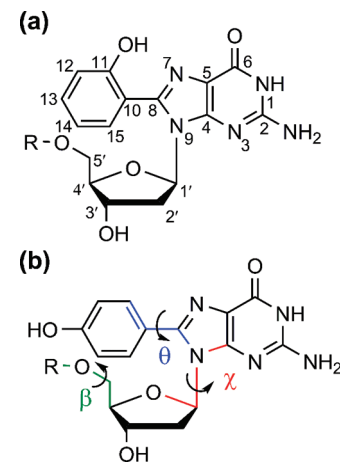


Figure 1. The structure and numbering of the (a) *ortho* and (b) *para* C8-phenoxy-2'-deoxyguanosine adduct nucleoside ($R = H$) and nucleotide ($R = PO_3^{2-}$, HPO_3^{2-} , or $Na^+ PO_3^{2-}$) models considered in the present work. The dihedral angle γ ($\angle(O4'-C1'-N9-C4)$) defines the glycosidic bond orientation to be *anti* ($\gamma = 180 \pm 90^\circ$) or *syn* ($\gamma = 0 \pm 90^\circ$), θ ($\angle(N9-C8-C10-C11)$) defines the degree of twist between the nucleobase and the bulky substituent, and β ($\angle(C4'-C5'-O-R)$) defines the orientation of the phosphate backbone in DNA.

react with the C8 site of guanine to form both covalent O- and C-bonded adducts.³⁶ In the present study, we consider phenolic adducts arising from C-attachment (Figure 1), which are structurally related to other C8-aryl-purine adducts of interest

* To whom correspondence should be addressed.

[†] University of Lethbridge.

[‡] University of Guelph.

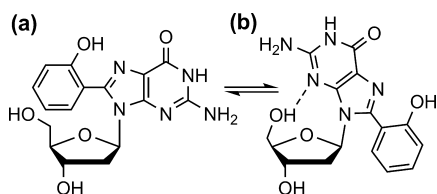


Figure 2. The (a) *anti* and (b) *syn* orientations of the *ortho*-C8-phenoxyl-2'-deoxyguanosine nucleoside adduct, where the preferred *syn* orientation contains a stabilizing C5'OH-H \cdots N3 hydrogen bond and the *anti* conformation is destabilized by the presence of the bulky substituent above the sugar moiety. See Figure 1 for atomic numbering.

in the current literature. For example, carcinogenic aryl hydrazines^{21,37–39} and polycyclic aromatic hydrocarbons (PAHs)⁴⁰ produce aryl radical intermediates that lead to C8-aryl adducts. Additionally, some natural phenolic toxins, such as ochratoxin A, can be activated to form C-bonded C8 adducts.^{20,36,41,42}

The first step toward understanding the biological consequences of C8-aryl-2'-deoxyguanosine adducts is to understand their structure. The bulky group in C8 adducts is positioned over the sugar moiety in the *anti* orientation ($\chi = 180 \pm 90^\circ$, Figure 1) preferred by all natural DNA nucleosides (Figure 2a).^{43,44} Therefore, many bulky C8 adducts prefer a *syn* orientation ($\chi = 0 \pm 90^\circ$, Figure 1) in B-DNA helices (Figure 2b),⁴⁵ which can lead to detrimental biological consequences. For example, the carcinogenic *N*-2-(2'-deoxyguanosine-8-yl)-acetylaminofluorene (G-AAF) lesion is known to exhibit frame-shift mutations due to the *syn* orientation,⁴⁶ while mutagenic studies report that the *syn* conformation adopted by *N*-(guanine-8-yl)-1-amino-6-nitropyrene and *N*-(guanine-8-yl)-1-amino-8-nitropyrene adducts disrupts base pairing.⁴⁷ Molecular dynamics simulations show that C8-phenyl-substituted adducts also prefer the *syn* orientation,²² and the C8-arylamine adducts are known to behave in an analogous fashion.²³ However, the *N*-(2'-deoxyguanosine-8-yl)-aminofluorene (G-AF) adduct is believed to readily adopt both the *syn* and *anti* conformations.^{46,48} These latter studies suggest that an *anti/syn* transition is possible when a bulky group is present, but preferential adoption of the *syn* orientation is not a foregone conclusion. Therefore, individual bulky C8 adducts need to be studied more closely to determine their structural preference, and the resulting mutagenicity.

In this light, we previously studied the *ortho* and *para* phenoxy nucleoside adducts ($R = H$, Figure 1) using a combined computational and experimental approach.²⁶ Our work shows that the bases in these modified nucleosides prefer a *syn* orientation about the glycosidic (N9–C1') bond (Figure 2b) due to the presence of a strong C5'OH-H \cdots N3 hydrogen bond, as well as the destabilization of the *anti* structure (Figure 2a) due to positioning of the bulky group directly above the sugar moiety.²⁶ However, it is not clear whether the preference of the nucleoside to adopt the *syn* structure applies to the DNA duplex, where the stabilizing C5'OH-H \cdots N3 hydrogen-bond contact is no longer possible due to the presence of a phosphate group at C5'. Indeed, previous literature suggests that the preference for the *anti* versus *syn* orientation in the natural nucleosides is dependent on the presence of intramolecular hydrogen bonds, as well as the computational model employed.^{49–53} Therefore, it may not be possible to extrapolate conclusions drawn for the nucleoside model to the physiological system.

The present study expands upon our previous work investigating the *anti/syn* preference of bulky DNA adducts by considering larger model systems that better mimic the environment in DNA helices. The nucleoside model is first adjusted

by including a geometric constraint, which prevents interactions between the base and the sugar moiety that cannot occur in the helix. Subsequently, the nucleoside model will be expanded to a nucleotide model by including the 5'-monophosphate group, which will also provide insight into the effect of potential interactions between the base and the DNA phosphate backbone on the conformational preference.

To the best of our knowledge, the *anti/syn* preference of only one bulky adduct has been studied using a nucleotide model.⁵⁴ Furthermore, computational modeling of the *anti/syn* preference of even the natural nucleotides has proven challenging,^{55–59} where the correct *anti/syn* energy trend for natural 2'-deoxyguanosine (dG) 5'-monophosphate has only been found using very specific computational models.⁶⁰ Since these models assume prior knowledge of the biologically relevant nucleotide conformation, which is unavailable for most damaged systems, these results cannot be applied to the DNA adducts of interest in the present work. Therefore, before studying the *anti/syn* energy difference for the *ortho* and *para* phenoxy adducts, we benchmark our computational approach by investigating natural 2'-deoxyguanosine 5'-monophosphate. Our studies of the structural preferences of the nucleoside and nucleotide adducts will aid in establishing a protocol for using small models to predict the preferred orientation of bulky damaged bases in physiological environments, as well as provide new information about the structure of C8-phenoxy adducts in B-DNA.

Computational Details

Nucleoside Model. To provide detailed information about the conformations available to the *ortho* and *para* nucleoside adducts ($R = H$, Figure 1), potential energy surfaces were generated in the gas phase at the B3LYP/6-31G(d) level of theory. Specifically, potential energy surface scans were previously performed, where the system was optimized with χ ($\angle(O4'-C1'-N9-C4)$) and θ ($\angle(N9-C8-C10-C11)$) angles (Figure 1) constrained in 10° increments from 0 to 360° .²⁶ In the present work, these surfaces will be compared to those generated using the same scanning procedure while imposing an additional constraint that fixes the $\angle(C4'-C5'-O-H)$ dihedral angle, which corresponds to the β ($\angle(C4'-C5'-O-P)$) angle in DNA (Figure 1), at 180° .⁶¹ This additional constraint prevents interactions between the base and the (C5'-OH) sugar that would not occur in natural (B-DNA) oligonucleotides. The former scans from our previous work will be referred to as the β -unconstrained surfaces, while the latter scans generated in the current study will be denoted as the β -constrained surfaces. Minimum energy conformations identified on the potential energy surfaces were subsequently optimized with no constraints at the B3LYP/6-31G(d) level. Accurate relative energies of these fully optimized structures were determined using B3LYP/6-311+G(2df,p) single-point calculations and include scaled (0.9806) zero-point vibrational energy (ZPVE) corrections.

Nucleotide Model. The nucleotide model was generated by adding the 5'-monophosphate group to the lowest energy *anti* and *syn* conformations identified using the (β -constrained) nucleoside model. As discussed in detail in the Results and Discussion, a variety of (neutral and charged) models were used to represent the phosphate group in DNA ($R = PO_3^-$, HPO_3 , or $Na^+ PO_3^-$, Figure 1). The natural dG nucleotide was also considered in order to ensure that biologically relevant structures were obtained with our various computational models. The natural nucleotide and *ortho* phenoxy adduct models were optimized with B3LYP and both the 6-31G(d) and 6-31+G(d,p) basis sets because of the potential importance of including

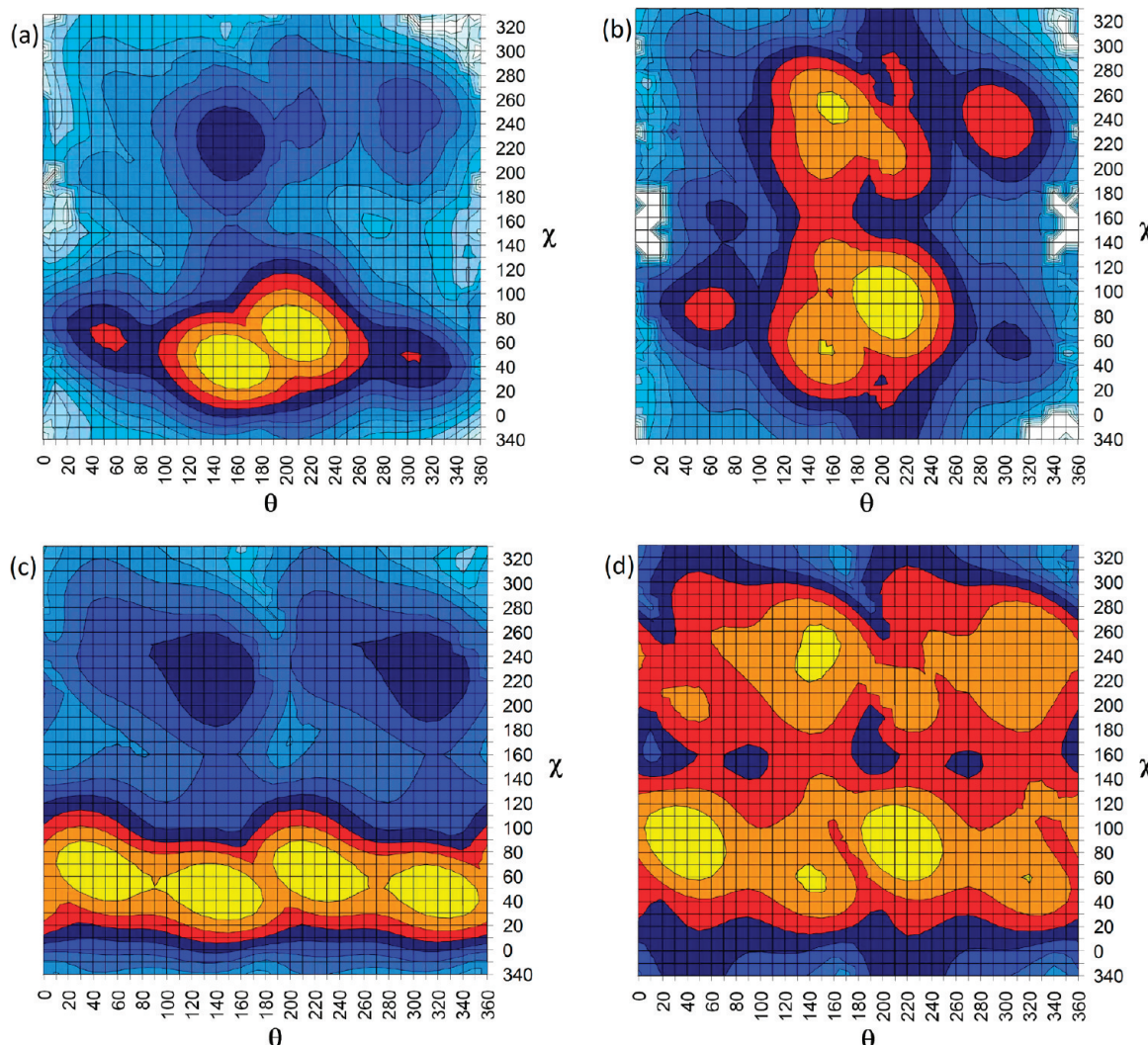


Figure 3. B3LYP/6-31G(d) potential energy surface for the (a) β -unconstrained *ortho* adduct,²⁶ (b) β -constrained *ortho* adduct, (c) β -unconstrained *para* adduct,²⁶ and (d) β -constrained *para* adduct. The relative energy is represented by color, where yellow represents the lowest energy regions, and each change in color represents an increase in the relative energy by 10 kJ mol⁻¹.

diffuse functions when considering models containing phosphate anions. Due to minimal differences between the geometries obtained for the *ortho* phenoxy adduct with the two basis sets (see Results and Discussion), the *para* phenoxy adduct was only considered at the B3LYP/6-31G(d) level of theory. All models were optimized in both the gas phase and in a water environment using the PCM continuum solvation model ($\epsilon = 78.4$). The reported relative energies, which include (0.9806) scaled ZPVE corrections, were obtained from B3LYP/6-311+G(2df,p) single-point calculations performed in the same (gas-phase or water) environment as the corresponding optimization.

All calculations were performed using Gaussian 03.⁶²

Results and Discussion

Nucleoside Model. The structures of C8-phenoxy-2'-deoxyguanosine nucleosides were previously investigated experimentally and computationally.²⁶ As found for other bulky C8-purine adducts^{21–23,45–48} (β -unconstrained), conformational scans (Figure 3a,c) reveal that *syn* minima ($\chi \sim 50–70^\circ$) of the *ortho* and *para* phenoxy C8-purine nucleoside adducts are favored over *anti* minima ($\chi \sim 230^\circ$) by 25–35 kJ mol⁻¹. Furthermore, the *syn* structures may potentially fit better into a B-DNA helix. In particular, the *syn* orientations have the correct (C2'-*endo*) sugar puckering, while the *anti* conformers prefer O4'-*endo*

puckering due to interactions between the bulky group and the sugar moiety. Additionally, the greater number of *syn* local minima with respect to the θ dihedral angle, which dictates the relative orientation of the natural base and the bulky substituent, suggests that the bulky group may twist with respect to the nucleobase as required to accommodate the helical environment.

Despite the energetic and conformational benefits of the *syn* structures discussed above, the possibility of adopting the (natural) *anti* conformation in DNA helices cannot be discounted based on our results. Specifically, as found for the natural nucleosides,^{51,52,63,64} the *syn* conformer of the adducts is stabilized by a strong C5'OH...N3 hydrogen bond (Figure 2b) that cannot occur in DNA due to the presence of the phosphodiester backbone. Therefore, models that better reflect the physiological environment are necessary to determine the effects of the bulky C8 group on the structural preference in B-DNA. This is initially accomplished in the present work by scanning the potential energy surfaces of the *ortho* and *para* phenoxy adducts with the β ($\angle(C4'-C5'-O-H)$) dihedral angle (see Figure 1) constrained to 180°, where this constraint has previously been used in the literature to study natural nucleosides.^{50,52,53,65–67}

Figure 3 compares the β -unconstrained (a and c) and β -constrained (b and d) potential energy surfaces of the phenoxy

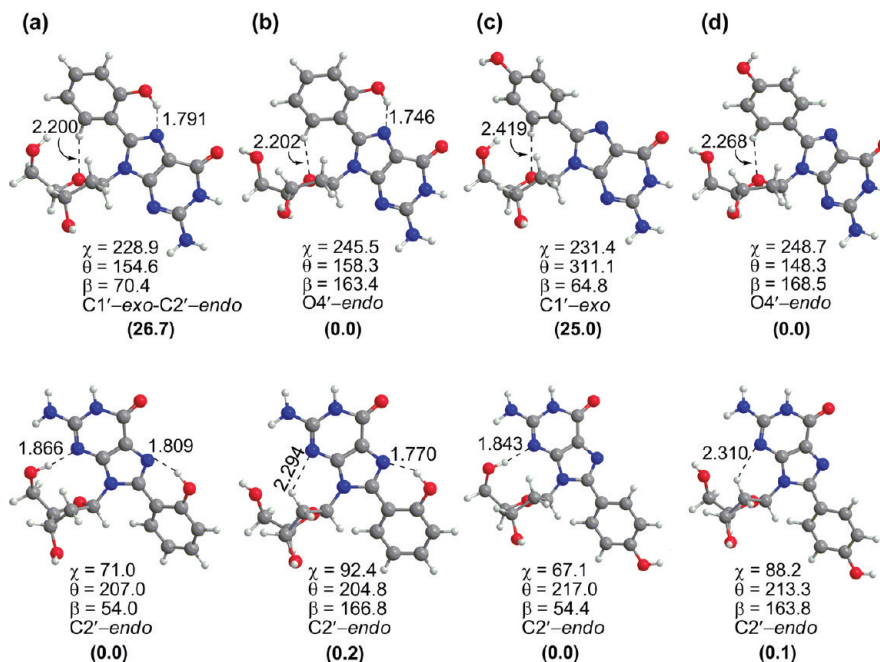


Figure 4. Select B3LYP/6-31G(d) hydrogen-bond lengths (\AA), dihedral angles (χ , θ , and β , deg.), and sugar puckering in the minimum energy (fully optimized) *anti* (top) and *syn* (bottom) structures obtained from the potential energy surfaces of the (a) β -unconstrained *ortho* adduct,²⁶ (b) β -constrained *ortho* adduct, (c) β -unconstrained *para* adduct,²⁶ and (d) β -constrained *para* adduct. (The *anti/syn* relative energies (kJ mol⁻¹) from B3LYP/6-311+G(2df,p) single-point calculations are provided in bold in parentheses.)

adducts.²⁶ The *syn* regions of the contour plots for the *ortho* and *para* phenoxy adducts are similar on both surfaces, where four *syn* minima can be identified for each adduct. For the *ortho* phenoxy adduct, the differences in the *anti* regions are also minimal. However, the change in the *anti* region is more significant for the *para* phenoxy adduct. Specifically, four *anti* minima are found on the β -constrained surface (Figure 3d), but only two are found on the β -unconstrained surface (Figure 3c). The two additional minima on the β -constrained surface correspond to rotation of the bulky phenoxy group about θ , which is impeded in the (β -unconstrained) nucleoside model when the C5'-OH group is directed toward the natural nucleobase. This indicates that the *para* phenoxy adduct may have greater flexibility in the *anti* conformation than initially predicted by our unconstrained nucleoside model, and therefore this orientation may be as readily accommodated in DNA helices as the *syn* conformer.

The most important feature of the potential energy surfaces (with and without the constraint on the C5'-OH group) is the relative energy of the *syn* and *anti* minima. Upon inclusion of the β constraint, the *anti* region becomes more energetically accessible for both adducts. For example, while the four *syn* minima of the *ortho* phenoxy adduct are all lower in energy than the two *anti* minima on the β -unconstrained surface (Figure 3a), the *anti* minima are lower in energy than two of the *syn* minima on the β -constrained surface (Figure 3b). Indeed, the *anti/syn* energy difference is 26 kJ mol⁻¹ (25 kJ mol⁻¹ for *para*) on the unconstrained surface, but only 7 kJ mol⁻¹ when the β -constraint is imposed. This indicates that the conformational energy trend is model dependent, and stresses the importance of considering models that better mimic the DNA environment when determining the conformational preference of damaged bases.

To further understand the *anti/syn* conformational preference, optimizations were performed with all constraints released for each minimum taken from the potential energy surfaces in Figure 3, where the resulting lowest energy *anti* and *syn* conformations for each adduct are displayed in Figure 4.⁶⁸ In

general, for both the *anti* and *syn* structures, χ and θ values deviate from the constrained geometries by less than 5°, while β typically deviates by less than 17°. The sugar puckering of the *syn* adducts usually remains in the (C2'-*endo*) form present in B-DNA,⁶⁹ while the lowest energy *anti* structures retain O4'-*endo* puckering. The C5'-OH group remains directed away from the nucleobase (Figure 4b,d) upon full optimization of the lowest energy conformers from the β -constrained surfaces.⁷⁰

The change in the relative energies of the *anti* and *syn* conformations upon geometry relaxation is more significant than any structural change. Specifically, the *anti* structures are all stabilized upon full optimization, which results in the lowest energy *anti* minima being almost energetically equivalent to the *syn* minima. In fact, *anti* minima are now the global minima on the surfaces (falling 0.1–0.2 kJ mol⁻¹ below the corresponding lowest energy *syn* structure). Since our results emphasize the dependence of the calculated *anti/syn* energy difference on the computational model, the lowest energy *syn* and *anti* conformations are further studied in the next section using a nucleotide model containing a 5'-monophosphate group.

Nucleotide Model. Despite drastic improvements in computational resources over the past decade, nucleotide models^{53,55,57,58,60,67,71–78} have not been studied in the literature to the same extent as nucleoside models.^{49,51,64,79–81} This is initially surprising since inclusion of the 5'-monophosphate group could clarify the conformational preference of DNA bases without drastically increasing the model size. However, the physiologically relevant *anti/syn* energy trends and geometries of nucleotides isolated by crystal structures⁸² and NMR^{65,83–85} have proven difficult to reproduce with computational methods. Specifically, similar to the nucleoside model, the phosphate group in nucleotide models can form interactions with nucleobases that are non-native to DNA.⁵³ Therefore, most computational studies that have reproduced the experimentally determined *anti/syn* preference for (natural) dG 5'-monophosphate, in particular, have imposed geometric constraints on the β angle,⁵³ where this angle is generally fixed to 180° to mimic

natural B-DNA helices.⁶¹ Although the use of constraints derived from structural databases is a successful approach for the canonical nucleotides, no geometrical parameters for the damaged nucleotides are known. Therefore, it is not surprising that even less has been done to study the structure of nucleotides modified by a bulky substituent. To the best of our knowledge, only one recent paper has studied the glycosidic-bond orientation in a bulky nucleotide adduct, which was an N7-substituted deoxyguanosine-like nucleotide.⁵⁴

Due to the absence of experimental data for comparison, a model for the natural dG nucleotide that correctly predicts the *anti/syn* preference without constraints must be identified before our systems of interest can be considered. Previous literature has used different approaches to model the structure of natural nucleotides without artificial constraints. Some groups have used dinucleotide monophosphate models to successfully reproduce experimental structural data, since the phosphate is anchored in position through attachment of the second sugar moiety.^{59,66,72} However, these models raise questions regarding the sequence dependence of the conformation.^{59,66,85} Although a B-DNA-like *syn* structure of dG 5'-monophosphate can be found in gas-phase studies that use large basis sets and/or high levels of theory,^{73,76} the correct energy trend is not predicted.⁷³ Furthermore, the computational methods employed are not suitable for studying larger (damaged) nucleotides. The first computational study to correctly predict the *anti/syn* preference of the natural 2'-deoxyguanosine 5'-mononucleotide without the use of constraints used a cationic model, where a magnesium ion complexed to four explicit water molecules is coordinated to N7 of guanine and thereby anchors the nucleotide in the *anti* conformation.⁶⁰ Although this model is valid for interpreting some enzyme active sites, it is not relevant for understanding the structures of DNA duplexes.

In addition to questions regarding the implementation of geometrical constraints, there are many different ways to model the DNA phosphate moiety, which can be represented by a variety of overall neutral and charged states. When the phosphate is modeled as a neutral (H_2PO_4^-) group, the preferred conformation is incorrectly predicted to be the *syn* orientation for all four natural nucleotides.^{55,58} Monoanionic phosphate models (HPO_4^{2-}) accurately predict 2'-deoxyadenosine 5'-monophosphate, 2'-deoxycytidine 5'-monophosphate, and thymidine 5'-monophosphate to be in the *anti* orientation, but consistently predict the *syn* orientation for 2'-deoxyguanosine 5'-monophosphate due to the presence of strong intramolecular hydrogen bonds between the base and the phosphate group.^{57,76,77} Even though this may be the preferred gas-phase conformation for this model, these results are not relevant to biological systems. Models that include sodium counterions to neutralize the phosphate group ($\text{Na}^+\text{HPO}_4^{2-}$) give a slightly better reproduction of crystal structure data due to a net zero charge in the crystals.^{72,75} Although dianionic phosphate models only describe *anti* minima for all four canonical nucleotides due to repulsion between the base and the phosphate group, the high net charge in the system makes these models unrealistic representations of DNA.⁵⁵ Therefore, the current study modeled dG 5'-monophosphate using the three most commonly accepted representations of the DNA phosphate backbone: a neutral (H_2PO_4^-) model, a neutral sodium counterion ($\text{Na}^+\text{HPO}_4^{2-}$) model, and an anionic (HPO_4^{2-}) model.

1. Gas-Phase Structure of the Natural dG Nucleotide. Although the discussion below focuses on the structure of the natural 2'-deoxyguanosine nucleotide obtained with the 6-31G(d) basis set, the same conclusions hold true for geometries obtained with 6-31+G(d,p), where the corresponding geometrical pa-

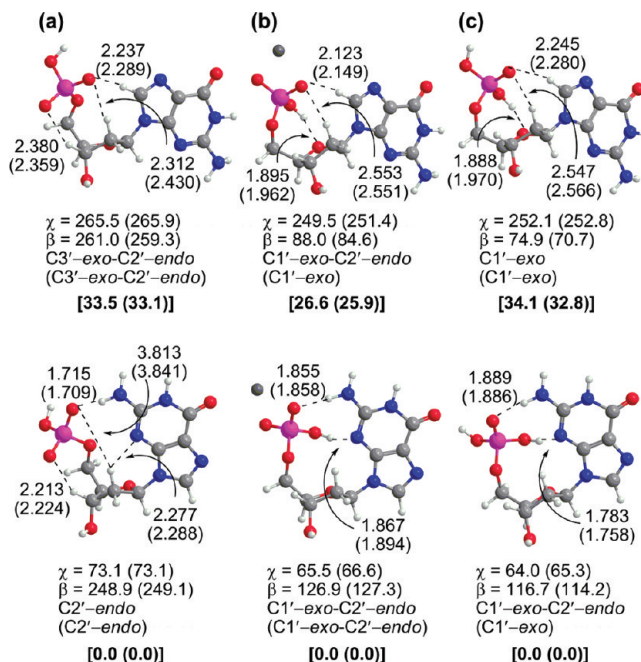


Figure 5. The *anti* (top) and *syn* (bottom) gas-phase structures of natural 2'-deoxyguanosine 5'-monophosphate described by the (a) anionic HPO_4^{2-} , (b) counterion $\text{Na}^+\text{HPO}_4^{2-}$, and (c) neutral H_2PO_4^- phosphate models. Select B3LYP/6-31G(d) hydrogen-bonds (Å), dihedral angles (χ and β , deg.), and sugar puckering are provided, where values for B3LYP/6-31+G(d,p) structures are provided in parentheses. B3LYP/6-31+G(2d,p) relative energies (kJ mol⁻¹) are in bold square brackets.

rameters are provided in parentheses in Figure 5. In all gas-phase structures (Figure 5), the additional proton on the phosphate group in the neutral model is not involved in interactions with the base or sugar moiety, and the only sodium interactions in the counterion model involve equivalent contacts with the two unprotonated oxygen atoms in the phosphate group ($\text{R}(\text{Na}^+\cdots \text{O}) \sim 2.2\text{--}2.4$ Å).

The three (gas-phase) *anti* structures (Figure 5, top) have χ angles between 250–265°, which are the values expected for B-DNA.⁴⁴ All three models form hydrogen bonds between C8-H in the base and a phosphate oxygen, as well as weaker interactions between C2'-H and the same phosphate oxygen. Both of these interactions have been previously reported in the literature.^{58,73} Similar interactions between the nucleobase and phosphate backbone occur in all models since χ is similar for the counterion and neutral models, and differs by only 13–16° for the anionic model. However, although the neutral and counterion models form similar hydrogen bonds between the phosphate and the sugar moiety, the anionic model differs considerably. Specifically, the β angle is rotated to 75–88° in the neutral and counterion models, which results in a non-native hydrogen bond between the terminal protonated phosphate oxygen and O4', while β is rotated in the opposite direction to 261° in the anionic model, which leads to interactions between the unprotonated phosphate oxygen and C3'-H in the sugar. These phosphate-sugar intramolecular interactions distort the B-DNA (C2'-endo) sugar puckering, where the anionic model exhibits a C3'-exo-C2'-endo twist, and the neutral and counterion models adopt a C1'-exo pucker.

For all three *syn* dG 5'-monophosphate models, the N2 amino group forms a hydrogen bond with an unprotonated phosphate oxygen (Figure 5, bottom), which is strongest (shortest) in the anionic model followed by the counterion model, as expected based on the relative charge on the phosphate in each model.

This contact is expected in B-DNA, and has been proposed to cause the *syn* orientation to be more stabilized for guanine than the other natural bases.^{53,67,73,74} The nucleoside model does not contain this native interaction, which emphasizes the importance of considering larger, more complete nucleotide models. As discussed for the *anti* orientation, the counterion and neutral models share similar χ values ($64\text{--}66^\circ$), while the anionic model differs by $8\text{--}9^\circ$. Consequently, the neutral and counterion models form a similar non-native hydrogen bond between the protonated phosphate oxygen and N3 of guanine (Figure 5b,c bottom), which is significantly shorter in the neutral model due to a 10° larger β angle. In contrast to these models, β (249°) rotates the phosphate group away from the nucleobase in the anionic model, which results in a hydrogen bond between the unprotonated phosphate oxygen and C3'-H of the sugar that is not expected in DNA.⁷³

As previously found in the literature^{55,56,58,73,76} our calculated relative energies for all nucleotide models predict a preferred *syn* orientation for 2'-deoxyguanosine 5'-monophosphate (Figure 5). The *syn* preference is large, ranging from $26.6\text{--}34.1\text{ kJ mol}^{-1}$. Although the calculated *syn* stability is similar for the neutral and anionic model, it is smaller for the counterion model. The same result is found with the larger (6-31+G(d,p)) basis set, where the difference in the *syn* preference between basis sets is less than 2 kJ mol^{-1} . Furthermore, for both basis sets, the *syn* geometry is distorted from the biologically relevant structure by the formation of non-native intramolecular hydrogen bonds. Therefore, our results demonstrate that gas-phase optimizations with these (double- ζ) basis sets do not yield the correct *anti/syn* energy trend, or structures relevant to B-DNA.

Other computational studies have reported that including the effects of the (implicit) water environment as an energy correction decreases the relative energy of the *anti* conformations of the natural nucleotides (but *syn* is still the preferred orientation).⁵⁶ Although inclusion of an energy correction alone cannot fix the structural problems reported in the present work, these previous results suggest that including the effects of solvation directly in the optimization routine may yield different minimum energy structures. Therefore, the effects of solvation on the structure of the nucleotide are considered in the next section by performing optimizations in a (bulk) water environment.

2. Effects of the Water Environment on the Structure of the Natural dG Nucleotide. The *anti* and *syn* conformers described by the three phosphate models were optimized in (implicit) water without imposing constraints on the backbone using the PCM continuum method with the 6-31G(d) and 6-31+G(d,p) basis sets (Figure 6). Water was chosen as the solvent since the gas-phase structures cannot correctly model the phosphate orientations in DNA helices and the phosphate backbone is highly solvated in DNA. The resulting *anti* structures for the three models (Figure 6, top) differ significantly from the corresponding gas-phase conformations (Figure 5, top). While the χ values deviate by 40° in the anionic model and 5° in the neutral and counterion models, the β angles are shifted (by $\sim 90^\circ$) to the range expected for B-DNA ($\sim 185^\circ$).⁶¹ Importantly, no interactions between the non-native terminal 5'-phosphate hydrogen and the base or sugar moiety are observed. Indeed, overall there are fewer and weaker intramolecular hydrogen bonds in the *anti* structures optimized in water compared to the gas-phase geometries. Our results indicate that, in a polar environment, intramolecular interactions between the phosphate and sugar do not exist, and that interactions between the phosphate and the base are not a significant source of stabilization. Additionally, unlike the gas phase, the *anti*

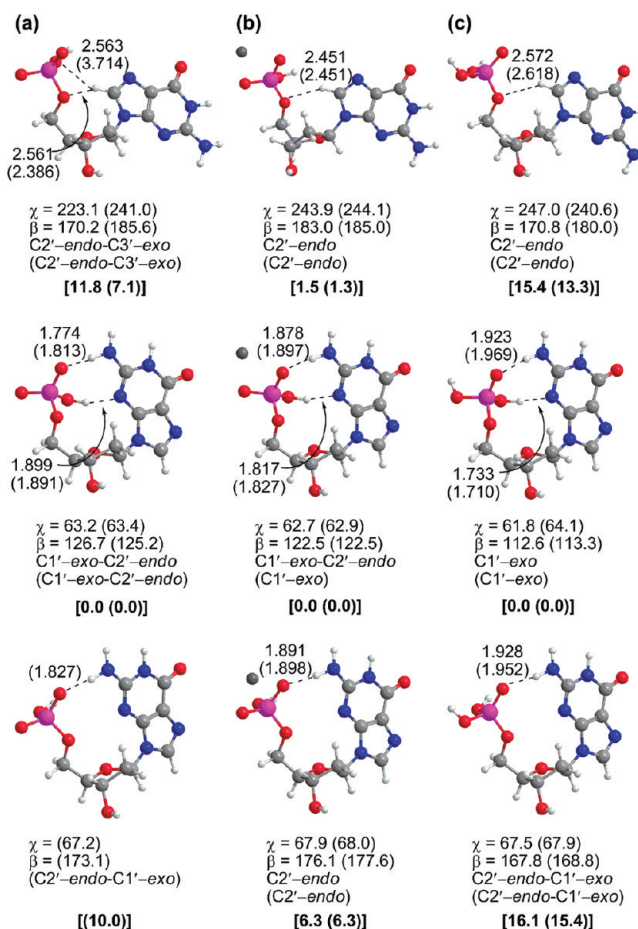


Figure 6. The *anti* (top), distorted *syn* (middle), and biologically relevant *syn* (bottom) structures optimized in water for natural 2'-deoxyguanosine 5'-monophosphate described by the (a) anionic HPO_4^{2-} , (b) counterion $\text{Na}^+ \text{HPO}_4^{2-}$, and (c) neutral H_2PO_4^- phosphate models. Select B3LYP/6-31G(d) hydrogen-bonds (\AA), dihedral angles (χ and β , deg.), and sugar puckering are provided, where values for B3LYP/6-31+G(d,p) structures are provided in parentheses. B3LYP/6-311+G(2df,p) relative energies (kJ mol^{-1}) are in bold square brackets.

conformation optimized in water has the B-DNA sugar puckering (C2'-endo).

Similar to the gas phase, a distorted *syn* orientation was optimized in water for all models (Figure 6, middle) with the phosphate group rotated toward the nucleobase ($\beta = 113\text{--}126^\circ$), and χ equal to $62\text{--}63^\circ$. Two hydrogen-bonding contacts are present in all three structures. First, a hydrogen bond between the N2 amino group of guanine and the phosphate oxygen was found. Although this interaction is also present in the gas-phase, all three models have weaker (longer) bonds in water than in the gas phase. Second, a hydrogen-bond contact between the protonated phosphate oxygen and N3 of guanine is observed. Although this interaction was previously found for the counterion and neutral models (not the anionic model) in the gas-phase, this interaction is stronger in water. This non-native hydrogen-bonding interaction renders these structures not relevant to DNA.

In addition to the distorted *syn* structures that are similar to those optimized in the gas phase, we characterized *syn* structures of biological interest in water, where the phosphate backbone orientation resembles that typically found in B-DNA⁶¹ (Figure 6, bottom). Specifically, the β values range from 168 to 176° and χ equals $67\text{--}68^\circ$. These geometrical parameters are also in good agreement with the previous large basis set gas-phase

study.⁷³ However, a modified anionic model was implemented in this previous study that avoids intramolecular interactions by protonating a phosphate oxygen not involved in the phosphodiester linkage to the neighboring nucleotide in B-DNA. Similar to the *anti* (water) orientations, no unnatural hydrogen bonds between the protonated phosphate oxygen and the nucleobase are found in the *syn* (water) structures. Thus, for the first time, a biologically relevant *syn* structure was characterized in the present work in the absence of constraints using a reasonably sized basis set suitable for studying bulky DNA adducts. The interaction between the amino group and the phosphate oxygen that is expected in DNA^{53,67,73,74} is still present in our models. Since this interaction is responsible for stabilizing the *syn* orientation of the nucleotide, this again highlights the importance of considering nucleotide models when attempting to understand the conformational preference in DNA. It should also be noted that the N2–H \cdots O–P hydrogen bond in the present study is weaker (1.8–1.9 Å) compared to the similar *syn* structure characterized in a previous gas-phase study (1.618 Å) using a modified anionic model.⁷³

As mentioned above, the structures of the natural nucleotides were studied with two basis sets (6-31G(d) and 6-31+G(d,p)). The geometries obtained with both basis sets generally deviate by up to 10° with the exception of two significant differences, which both occur for the anionic water model. First, the *anti* anionic structures have different intramolecular hydrogen bonds since γ deviates by 18° and β by 15°. For the smaller basis set, this leads to a bifurcated hydrogen bond between C8–H and a phosphate oxygen and O5' (Figure 6a, top), while the larger basis set results in a more direct hydrogen bond between C8–H and O5'. The second major difference is that no biologically relevant *syn* structure is obtained for the anionic model (in water) with the smaller (6-31G(d)) basis set. This stresses the importance of including diffuse functions in the basis set in order to accurately describe charged models. Furthermore, this discrepancy suggests that the anionic model cannot be reliably used in instances where the size of the nucleobase prohibits the use of a larger basis set. Thus, the anionic model may not be suitable for studying bulky DNA adducts.

In addition to characterizing biologically relevant *syn* conformations, consideration of solvated structures changes important conclusions regarding the *anti/syn* energy trend. Specifically, for all three models, the nonbiologically relevant *syn* orientation that is similar to the gas-phase structure remains the global minimum by 1–15 kJ mol⁻¹ (Figure 6). However, when the nucleotide conformation in DNA is of interest, this structure must be discarded and the most fair *anti/syn* energy difference is obtained by considering the biologically relevant *syn* minimum, which is only characterized in solvent-phase (water) optimizations.

At the B3LYP/6-31+G(d,p) level of theory, the biologically relevant *syn* structure is higher in energy than the *anti* conformation by 2–5 kJ mol⁻¹ for all three models (Figure 6, parentheses). Therefore, all three models correctly predict that *anti* is the preferred orientation about the glycosidic bond. At the B3LYP/6-31G(d) level of theory, the neutral and counterion models also predict the *anti* orientation to be lower in energy than the *syn* conformation by 0.7 and 4.8 kJ mol⁻¹, respectively. This is the first time the correct *anti/syn* energy trend has been computationally reproduced using an unconstrained nucleotide model for natural 2'-deoxyguanosine 5'-monophosphate. We note that the exaggerated N2–H \cdots O–P interaction partially explains why previous work predicted the incorrect *anti/syn* energy trend,⁷³ where this error could have been caused by the

basis set and/or the charged (anionic) model previously implemented. Although the structure in the present study is similar to the previous gas-phase structures,^{73,76} small differences in the geometric parameters (i.e., hydrogen-bond lengths) are clearly important for determining the correct *anti/syn* preference. Therefore, our solvated structures provide a more accurate representation of the dG nucleotide than has been previously reported in the literature. Our results stress the importance of including the effects of the (bulk) environment directly in the optimization routine, and that this approach has the same effect as adding geometric constraints, while still permitting a free optimization. Our new approach will be particularly useful when studying damaged or modified bases with unknown geometries.

Although the larger (smaller) basis set correctly predicts the *anti* conformer to be lower in energy than *syn* for all three (two) of the phosphate models considered in the present work, there are important discrepancies in the *anti/syn* energetic differences that differentiate the models. First, the *anti* preference predicted by both basis sets is largest for the counterion model. Second, the preference for the hydrogen-bonded *syn* structure calculated by both basis sets is smallest for the counterion model. We also found that the biologically relevant *syn* conformation is most readily optimized (i.e., has fewer convergence issues) when the counterion model is implemented with either basis set. The fact that the counterion model more reliably identifies a biologically relevant *syn* structure for the natural nucleotide with both basis sets suggests that this model should be implemented when modeling DNA nucleotides. This conclusion is especially true when smaller basis sets are implemented for computational efficiency. Therefore, due to the size of bulky DNA adducts, future studies of these nucleotides in geometries relevant to B-DNA should be conducted using the counterion model and incorporating bulk solvent effects in the optimization routine.

3. Structure of the *ortho* C8-phenoxy dG Nucleotide Adduct. Since it was shown that the counterion model more reliably reproduces biologically relevant structures and the *anti/syn* energetic preference for natural 2'-deoxyguanosine, this model will be employed to study the C8-phenoxy DNA adduct. However, since the majority of work in the literature uses neutral and anionic nucleotide models,^{52–59,66,67,73,74,76,77} these models will also be applied to the C8-phenoxy adducts to further illustrate why they should not be used to study damaged nucleotide conformations. The *ortho* C8-phenoxy-2'-deoxyguanosine 5'-monophosphate adduct was also optimized with both basis sets (6-31G(d) and 6-31+G(d,p)) to verify that the basis set effects are also small for damaged nucleotides, where interactions between the bulky group and the phosphate could occur. Indeed, we find that the differences between the two basis sets are negligible (Figure 7), and therefore only the results for the 6-31G(d) basis set will be discussed below unless otherwise indicated. Because of the clear importance of directly including (bulk) environmental effects in the optimization routine, all structures of the DNA adducts were optimized in water.

The optimized *anti* structures of the *ortho* phenoxy adduct with all models are very similar (Figure 7, top). The γ dihedral angle (\sim 245°) is close to our calculated values for the natural nucleotide (223–247°). Similarly, the β -dihedral angle varies only slightly across models (176–188°), and is shifted by only 5° in the neutral and counterion model and 15° in the anionic model compared with the natural nucleotide. Interestingly, the bulky group forms a weak C14–H \cdots O hydrogen bond with the phosphate group in the *anti* orientation, which is similar to the C8–H \cdots O interaction discussed in the *anti* natural nucleotide (Figure 6, top). A second weak C15–H \cdots O hydrogen

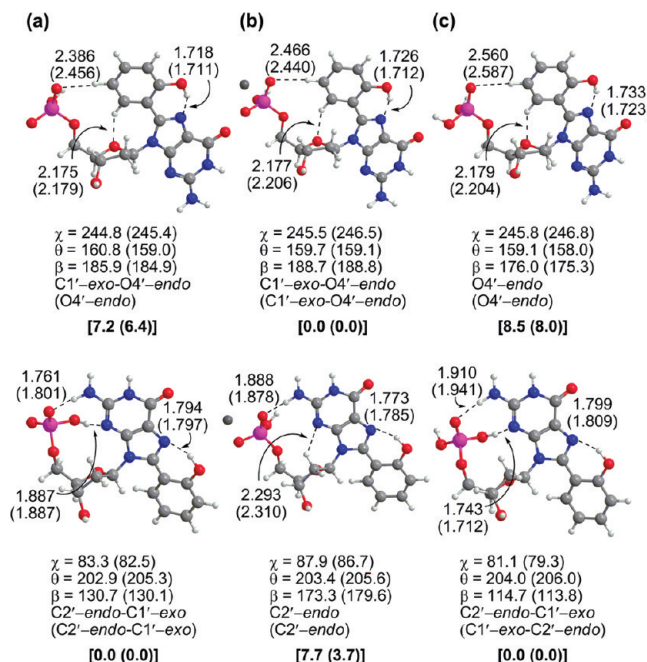


Figure 7. The *anti* (top) and *syn* (bottom) conformations of *ortho* C8-phenoxyl-2'-deoxyguanosine 5'-monophosphate described by the (a) anionic HPO_4^{2-} , (b) counterion $\text{Na}^+ \text{HPO}_4^{2-}$, and (c) neutral H_2PO_4^- phosphate models. Select B3LYP/6-31G(d) hydrogen-bonds (\AA), dihedral angles (χ and β , deg.), and sugar puckering are provided, where values for B3LYP/6-31+G(d,p) structures are provided in parentheses. B3LYP/6-311+G(2df,p) relative energies (kJ mol^{-1}) are in bold square brackets.

bond also forms with the sugar. This leads to the only significant difference in the *anti* structures, which is a change in the sugar puckering to become more O4'-*endo* upon damage. This interaction with the phosphate group represents a significant difference between the nucleoside and nucleotide models, which re-emphasizes the importance of considering larger models to understand DNA structure where phosphate interactions may become important in the helical environment.

In the *syn* structures of the *ortho* phenoxy adduct (Figure 7, bottom), the sugar puckering (C2'-*endo* or C2'-*endo*-C1'-*exo*) remains approximately the same as for the natural nucleotide. Each model also exhibits a hydrogen bond between the N2 guanine amino group and the phosphate oxygen, which is much stronger than the C-H \cdots O interactions observed in the *anti* orientation. Nevertheless, there are some major differences between the models. Specifically, although χ increases by 20° and β increases by 2–4° relative to the natural *syn* nucleotide for the neutral and anionic models, these models only characterize the non-native, hydrogen-bonded *syn* orientation discussed for the natural nucleotide in both the gas-phase and water. Indeed, the biologically relevant *syn* structure was not optimized with the anionic and neutral models using either basis set. However, the counterion model readily characterizes the biologically relevant *syn* structure with both basis sets, which involves deviations in β and χ by 3° and 20°, respectively, compared to the corresponding natural conformation. Furthermore, the hydrogen-bonded *syn* structure was not found for the counterion model. Thus, comparison of the structures optimized with all three models reinforces our previous conclusion that the counterion model is the best choice for modeling natural and damaged B-DNA nucleotides. In addition, the agreement between both basis sets confirms that the *para* phenoxy adduct can be studied at only the B3LYP/6-31G(d) level of theory.

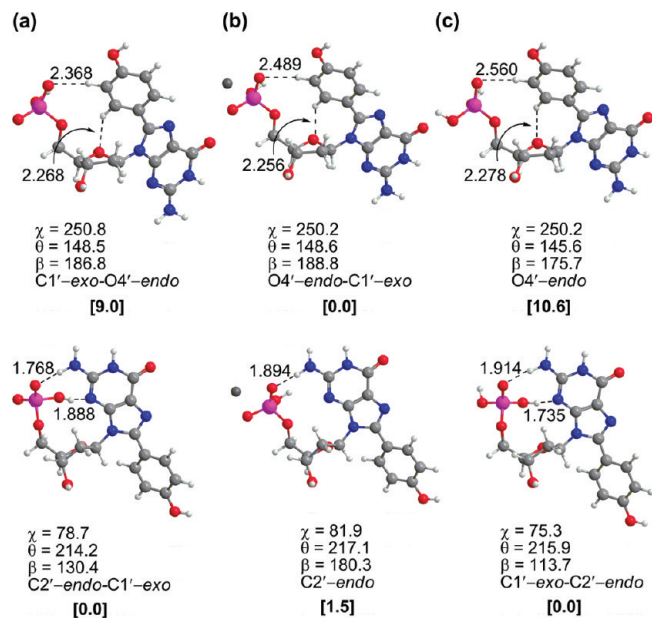


Figure 8. The *anti* (top) and *syn* (bottom) conformations of *para* C8-phenoxyl-2'-deoxyguanosine 5'-monophosphate described by the (a) anionic HPO_4^{2-} , (b) counterion $\text{Na}^+ \text{HPO}_4^{2-}$, and (c) neutral H_2PO_4^- phosphate models. Select B3LYP/6-31G(d) hydrogen-bonds (\AA), dihedral angles (χ and β , deg.), and sugar puckering are provided, where values for B3LYP/6-31+G(d,p) structures are provided in parentheses. B3LYP/6-311+G(2df,p) relative energies (kJ mol^{-1}) are in bold square brackets.

Although the neutral and anionic models predict the non-native hydrogen-bonded *syn* conformation to be energetically preferred as discussed for the natural nucleotide, the calculated energy difference between the *anti* and non-native *syn* orientations is smaller for the *ortho* phenoxy adduct (Figure 7). More importantly, the biologically relevant *syn* structure isolated using the counterion model is less stable than the *anti* orientation as discussed for the natural nucleotide. Interestingly, the energetic preference for the *anti* conformation is larger for the *ortho* phenoxy adduct (7.7 kJ mol^{-1}) than the natural nucleotide (4.8 kJ mol^{-1}). This suggests that the *ortho* phenoxy adduct will adopt the *anti* orientation in B-DNA, and therefore the *ortho* phenoxy adduct should behave like natural dG in terms of the base-pairing preference in DNA helices.⁸⁶ Nevertheless, the predicted preference for *anti* is small, and therefore both the *anti* and *syn* orientations of the damaged base are likely to be in equilibrium in the DNA helix. We also acknowledge that other environmental factors in the helix (such as stacking interactions, hydrogen-bonding interactions or groove contacts) may influence the preferred conformation.

4. Structure of the *para* C8-phenoxyl dG Nucleotide Adduct. As discussed above, the structural differences for any given conformation of the *ortho* phenoxy adduct obtained with the two basis sets are less than 6° (Figure 7) and the same conclusions are obtained regardless of the basis set implemented. Consequently, the *para* phenoxy adduct was only studied using the smaller (6-31G(d)) basis set. The *anti* structures of the *para* phenoxy adduct optimized with all models are very similar (Figure 8, top). The χ dihedral angle ($\sim 250^\circ$) is shifted by only 5° compared with the *ortho* phenoxy adduct, while the β -dihedral angles (175 – 188°) and sugar puckering (O4'-*endo*-C1'-*exo*) are identical for both adducts. A C14-H \cdots O interaction between the bulky phenoxy group and the phosphate is present, which again stresses the importance of considering nucleotide models. As discussed for the *ortho* adduct, only the

non-native hydrogen-bonded *syn* structure was characterized using the neutral and anionic models, while the biologically relevant *syn* conformation is only obtained for the counterion model. This finding once again confirms our recommendation of using this model in future studies. The *para* structures predicted with the counterion model differ from the *ortho* structures by only 7° in the β angle and 5° in χ , but the *para* phenoxy adduct lacks the interaction between N3 and C2'-H noted for the *ortho* adduct.

As discussed for the *ortho* phenoxy nucleotide adduct, the biologically relevant *syn* structure isolated using the counterion model leads to a preference for the *anti* orientation for the *para* phenoxy adduct (Figure 8). However, while the energetic preference for *anti* is greater for the *ortho* phenoxy adduct (7.7 kJ mol⁻¹) than the natural nucleotide (4.8 kJ mol⁻¹), the preference for *anti* is actually less for the *para* phenoxy adduct (1.5 kJ mol⁻¹). Therefore, the *anti* orientation is destabilized for the *para* phenoxy adduct relative to the natural base, and the very small energy difference suggests that the *syn* orientation could be adopted in B-DNA helices. This implies that the preferred nucleobase orientation in C8-phenoxy nucleotide adducts in B-DNA duplexes may depend on the relative location of the hydroxyl substituent.

Although the energy differences calculated in the present work are too small to conclusively determine whether there is a preferred base orientation in DNA, potential differences in the relative populations of the *anti* and *syn* conformations imply that the mutagenic potential of related bulky adducts may differ. Specifically, Hoogsteen interactions have the potential to be enhanced by the addition of the bulky substituent to C8^{87,88} when nucleotides adopt the *syn* orientation. In fact, if the Hoogsteen face of either the *ortho* or *para* phenoxy adduct forms a particularly stabilizing hydrogen-bonded pair with a natural base, the strength of the interaction may be sufficient to anchor the base in the *syn* orientation. Thus, our small calculated *anti/syn* energy differences imply that both conformations of the adduct may be observed in DNA, and that intermolecular interactions may participate in the stabilization of the adduct conformation in DNA.

Conclusions

The *anti/syn* conformational preference of the *ortho* and *para* C8-phenoxy-2'-deoxyguanosine nucleotide adducts was investigated in the present work. Similar to previously studied bulky C8-dG lesions, fully optimized nucleoside models predict the *syn* orientation to be favored due to the presence of a non-native strong C5'O-H \cdots N3 hydrogen bond. When an additional geometric constraint is imposed that prevents this interaction, the *syn* conformation becomes less important than initially predicted. Therefore, although the nucleoside model is popular in the literature and can provide some useful information regarding the structure of damaged bases, this model is insufficient to determine the *anti/syn* conformational preference of modified nucleobases in DNA.

To better predict the structure of the damaged bases in DNA helices, a nucleotide model that includes the 5'-monophosphate group was studied. However, since previous work could not predict the correct *anti/syn* preference for the natural dG nucleotide with a computational methodology suitable for bulky adducts, we first developed a model for the accurate treatment of the dG nucleotide. Our results confirm that biologically relevant *syn* conformations are characterized only when the effects of the (bulk) environment are taken into account during the optimization routine. Most importantly, the *syn* conformation is accurately determined to be less stable than the *anti*

conformation, which is most reliably predicted by the counterion model. This is the first time the correct conformational trend was calculated for natural 2'-deoxyguanosine 5'-monophosphate without the use of artificial geometric constraints.

The methodology used for the natural nucleotide was subsequently applied to the (damaged) *ortho* and *para* C8-phenoxy-2'-deoxyguanosine 5'-monophosphate adducts. Although both types of damage show a preference for the *anti* conformation, it is likely that both the *anti* and *syn* conformations will exist in equilibrium in the helix, which is similar to the conclusion for other closely related adducts. Furthermore, our calculations suggest that other sources of stabilization (such as hydrogen-bonding ability or steric clashes) may play an important role in determining the overall structure of damaged DNA helices and the relative populations of each conformer. Therefore, investigations that consider other properties of the adducts, including their hydrogen-bonding ability, and the structures of larger DNA oligomers are currently being conducted in our lab.

Acknowledgment. We thank the Natural Sciences and Engineering Research Council (NSERC), the Canada Foundation for Innovation (CFI) and the Canada Research Chair (CRC) program for financial support. A.L.M. thanks NSERC, Alberta Ingenuity (AIF), the Alberta government, and the University of Lethbridge for graduate student scholarships.

Supporting Information Available: Coordinates for all nucleotides in water. This material is available free of charge via the Internet at <http://pubs.acs.org>.

References and Notes

- (1) Lynch, S. R.; Liu, H. B.; Gao, J. M.; Kool, E. T. *J. Am. Chem. Soc.* **2006**, *128*, 14704–14711.
- (2) Ogawa, A. K.; Abou-Zied, O. K.; Tsui, V.; Jimenez, R.; Case, D. A.; Romesberg, F. E. *J. Am. Chem. Soc.* **2000**, *122*, 9917–9920.
- (3) Leumann, C. *J. Bioorg. Med. Chem.* **2002**, *10*, 841–854.
- (4) Sun, K. M.; McLaughlin, C. K.; Lantero, D. R.; Manderville, R. A. *J. Am. Chem. Soc.* **2007**, *129*, 1894–1895.
- (5) Greco, N. J.; Tor, Y. *Tetrahedron* **2007**, *63*, 3515–3527.
- (6) Bardon, A. B.; Wetmore, S. D. *J. Phys. Chem. A* **2005**, *109*, 262–272.
- (7) Greco, N. J.; Tor, Y. *J. Am. Chem. Soc.* **2005**, *127*, 10784–10785.
- (8) Srivatsan, S. G.; Greco, N. J.; Tor, Y. *Angew. Chem., Int. Ed.* **2008**, *47*, 6661–6665.
- (9) Polak, M.; Seley, K. L.; Plavec, J. *J. Am. Chem. Soc.* **2004**, *126*, 8159–8166.
- (10) Endo, M.; Sugiyama, H. *ChemBioChem* **2009**, *10*, 2420–2443.
- (11) Kool, E. T. *Acc. Chem. Res.* **2002**, *35*, 936–943.
- (12) Halliwell, B. *J. Neurochem.* **2006**, *97*, 1634–1658.
- (13) Nakabeppe, Y.; Tsuchimoto, D.; Yamaguchi, H.; Sakumi, K. *J. Neurosci. Res.* **2007**, *85*, 919–934.
- (14) Lu, A. L.; Li, X.; Gu, Y.; Wright, P. M.; Chang, D.-Y. *Cell Biochem. Biophys.* **2001**, *35*, 141–170.
- (15) Dizdaroglu, M. *Mutat. Res.* **2005**, *591*, 45–59.
- (16) Labahn, J.; Scherer, O. D.; Long, A.; EzazNikpay, K.; Verdine, G. L.; Ellenberger, T. E. *Cell* **1996**, *86*, 321–329.
- (17) Drablos, F.; Feyzi, E.; Aas, P. A.; Vaagbo, C. B.; Kavli, B.; Brattlie, M. S.; Pena-Diaz, J.; Otterlei, M.; Slupphaug, G.; Krokan, H. E. *DNA Repair* **2004**, *3*, 1389–1407.
- (18) Gates, K. S.; Noonan, T.; Dutta, S. *Chem. Res. Toxicol.* **2004**, *17*, 839–856.
- (19) Dai, J.; Wright, M. W.; Manderville, R. A. *Chem. Res. Toxicol.* **2003**, *16*, 817–821.
- (20) Dai, J.; Wright, M. W.; Manderville, R. A. *J. Am. Chem. Soc.* **2003**, *125*, 3716–3717.
- (21) Gannett, P. M.; Lawson, T.; Miller, M.; Thakkar, D. D.; Lord, J. W.; Yau, W. M.; Toth, B. *Chem. Biol. Interact.* **1996**, *101*, 149–164.
- (22) Heavner, S.; Gannett, P. M. *J. Biomol. Struct. Dyn.* **2005**, *23*, 203–219.
- (23) Stover, J. S.; Ciobanu, M.; Cliffel, D. E.; Rizzo, C. J. *J. Am. Chem. Soc.* **2007**, *129*, 2074–2081.

- (24) Biomarkers of Environmentally Associated Disease: Technologies, Concepts and Perspectives, 1st ed.; Wilson, S. H., Suk, W. A., Eds.; Lewis Publishers, CRC Press LLC: Boca Raton, FL, 2002.
- (25) Manini, P.; De Palma, G.; Andreoli, R.; Marczyński, B.; Hanova, M.; Mozzoni, P.; Naccarati, A.; Vodickova, L.; Hlavac, P.; Mutti, A.; Vodicka, P. *Toxicol. Lett.* **2009**, *190*, 41–47.
- (26) Millen, A. L.; McLaughlin, C. K.; Sun, K. M.; Manderville, R. A.; Wetmore, S. D. *J. Phys. Chem. A* **2008**, *112*, 3742–3753.
- (27) Manderville, R. A. *Chem. Res. Toxicol.* **2005**, *18*, 1091–1097.
- (28) Perry, J. L.; Il'ichev, Y. V.; Kempf, V. R.; McClendon, J.; Park, G.; Manderville, R. A.; Ruker, F.; Dockal, M.; Simon, J. D. *J. Phys. Chem. B* **2003**, *107*, 6644–6647.
- (29) Pfohl-Leszkowicz, A.; Manderville, R. A. *Mol. Nutr. Food Res.* **2007**, *51*, 61–99.
- (30) Tozlovanu, M.; Faucet-Marquis, V.; Pfohl-Leszkowicz, A.; Manderville, R. A. *Chem. Res. Toxicol.* **2006**, *19*, 1241–1247.
- (31) Dai, J.; Sloat, A. L.; Wright, M. W.; Manderville, R. A. *Chem. Res. Toxicol.* **2005**, *18*, 771–779.
- (32) Kato, T.; Kojima, K.; Hiramoto, K.; Kikugawa, K. *Mutat. Res.* **1992**, *268*, 105–114.
- (33) McLaughlin, C. K.; Lantero, D. R.; Manderville, R. A. *J. Phys. Chem. A* **2006**, *110*, 6224–6230.
- (34) Weishar, J. L.; McLaughlin, C. K.; Baker, M.; Gabryelski, W.; Manderville, R. A. *Org. Lett.* **2008**, *10*, 1839–1842.
- (35) Calcutt, M. W.; Gillman, I. G.; Nofle, R. E.; Manderville, R. A. *Chem. Res. Toxicol.* **2001**, *14*, 1266–1272.
- (36) Manderville, R. A. *Can. J. Chem. - Rev. Can. Chim.* **2005**, *83*, 1261–1267.
- (37) Kikugawa, K.; Kato, T.; Kojima, K. *Mutat. Res.* **1992**, *268*, 65–75.
- (38) Hiramoto, K.; Kojima, K.; Kato, T.; Kikugawa, K. *Mutat. Res.* **1992**, *272*, 259–260.
- (39) Gannett, P. M.; Heavner, S.; Daft, J. R.; Shaughnessy, K. H.; Epperson, J. D.; Greenbaum, N. L. *Chem. Res. Toxicol.* **2003**, *16*, 1385–1394.
- (40) Dai, Q.; Xu, D. W.; Lim, K.; Harvey, R. G. *J. Org. Chem.* **2007**, *72*, 4856–4863.
- (41) Faucet, V.; Pfohl-Leszkowicz, A.; Dai, J.; Castegnaro, M.; Manderville, R. A. *Chem. Res. Toxicol.* **2004**, *17*, 1289–1296.
- (42) Mantle, P. G.; Faucet-Marquis, F.; Manderville, R. A.; Squillaci, B.; Pfohl-Leszkowicz, A. *Chem. Res. Toxicol.* **2010**, *23*, 89–98.
- (43) Bloomfield, V. A.; Crothers, D. M.; Tinoco, I., Jr. *Nucleic Acids Structures, Properties, and Functions*; University Science Press: Mill Valley, CA, 2000.
- (44) The glycosidic bond angle (see Figure 1) in natural B-DNA is typically $252 \pm 23^\circ$, which represents an *anti* orientation (see ref 52).
- (45) Eason, R. G.; Burkhardt, D. M.; Phillips, S. J.; Smith, D. P.; David, S. S. *Nucleic Acids Res.* **1996**, *24*, 890–897.
- (46) Burnouf, D. Y.; Wagner, J. E. *J. Mol. Biol.* **2009**, *386*, 951–961.
- (47) Hilario, P.; Yan, S. X.; Hingerty, B. E.; Broyde, S.; Basu, A. K. *J. Biol. Chem.* **2002**, *277*, 45068–45074.
- (48) Watt, D. L.; Utzat, C. D.; Hilario, P.; Basu, A. K. *Chem. Res. Toxicol.* **2007**, *20*, 1658–1664.
- (49) Hocquet, A.; Leulliot, N.; Ghomi, M. *J. Phys. Chem. B* **2000**, *104*, 4560–4568.
- (50) Foloppe, N.; MacKerell, A. D. *J. Phys. Chem. B* **1999**, *103*, 10955–10964.
- (51) Shishkin, O. V.; Pelmenschikov, A.; Hovorun, D. M.; Leszczynski, J. *J. Mol. Struct.* **2000**, *526*, 329–341.
- (52) Foloppe, N.; Nilsson, L.; MacKerell, A. D. *Biopolymers* **2001**, *61*, 61–76.
- (53) Foloppe, N.; Hartmann, B.; Nilsson, L.; MacKerell, A. D. *Biophys. J.* **2002**, *82*, 1554–1569.
- (54) Kosenkov, D.; Kholod, Y. A.; Gorb, L.; Shishkin, O. V.; Kuramshina, G. M.; Dovbeshko, G. I.; Leszczynski, J. *J. Phys. Chem. A* **2009**, *113*, 9386–9395.
- (55) Gorb, L.; Shishkin, O.; Leszczynski, J. *J. Biomol. Struct. Dyn.* **2005**, *22*, 441–454.
- (56) Palamarchuk, G. V.; Shishkin, O. V.; Gorb, L.; Leszczynski, J. *J. Biomol. Struct. Dyn.* **2009**, *26*, 653–661.
- (57) Shishkin, O. V.; Gorb, L.; Zhikol, O. A.; Leszczynski, J. *J. Biomol. Struct. Dyn.* **2004**, *21*, 537–553.
- (58) Shishkin, O. V.; Gorb, L.; Zhikol, O. A.; Leszczynski, J. *J. Biomol. Struct. Dyn.* **2004**, *22*, 227–243.
- (59) Svozil, D.; Sponer, J. E.; Marchan, I.; Peñérez, A.; Cheatham, T. E., III; Forti, F.; Luque, F. J.; Orozco, M.; Sponer, J. i. *J. Phys. Chem. B* **2008**, *112*, 8188–8197.
- (60) Kosenkov, D.; Gorb, L.; Shishkin, O. V.; Sponer, J.; Leszczynski, J. *J. Phys. Chem. B* **2008**, *112*, 150–157.
- (61) The β angle in B-DNA is typically $168 \pm 25^\circ$ (see ref 52).
- (62) Frisch, M. J.; Trucks, G. W.; Schlegel, H. B.; Scuseria, G. E.; Robb, M. A.; Cheeseman, J. R.; Montgomery, J. A., Jr.; Vreven, T.; Kudin, K. N.; Burant, J. C.; Millam, J. M.; Iyengar, S. S.; Tomasi, J.; Barone, V.; Mennucci, B.; Cossi, M.; Scalmani, G.; Rega, N.; Petersson, G. A.; Nakatsuji, H.; Hada, M.; Ehara, M.; Toyota, K.; Fukuda, R.; Hasegawa, J.; Ishida, M.; Nakajima, T.; Honda, Y.; Kitao, O.; Nakai, H.; Klene, M.; Li, X.; Knox, J. E.; Hratchian, H. P.; Cross, J. B.; Bakken, V.; Adamo, C.; Jaramillo, J.; Gomperts, R.; Stratmann, R. E.; Yazyev, O.; Austin, A. J.; Cammi, R.; Pomelli, C.; Ochterski, J. W.; Ayala, P. Y.; Morokuma, K.; Voth, G. A.; Salvador, P.; Dannenberg, J. J.; Zakrzewski, V. G.; Dapprich, S.; Daniels, A. D.; Strain, M. C.; Farkas, O.; Malick, D. K.; Rabuck, A. D.; Raghavachari, K.; Foresman, J. B.; Ortiz, J. V.; Cui, Q.; Baboul, A. G.; Clifford, S.; Cioslowski, J.; Stefanov, B. B.; Liu, G.; Liashenko, A.; Piskorz, P.; Komaromi, I.; Martin, R. L.; Fox, D. J.; Keith, T.; Al-Laham, M. A.; Peng, C. Y.; Nanayakkara, A.; Challacombe, M.; Gill, P. M. W.; Johnson, B.; Chen, W.; Wong, M. W.; Gonzalez, C.; Pople, J. A. *Gaussian 03, Revisions C.02 and D.01*; Gaussian, Inc.: Wallingford, CT, 2004.
- (63) Foloppe, N.; MacKerell, A. D. *J. Phys. Chem. B* **1998**, *102*, 6669–6678.
- (64) Foloppe, N.; Nilsson, L. *J. Phys. Chem. B* **2005**, *109*, 9119–9131.
- (65) Sarma, R. H.; Lee, C. H.; Evans, F. E.; Yathindra, N.; Sundaral, M. *J. Am. Chem. Soc.* **1974**, *96*, 7337–7348.
- (66) MacKerell, A. D. *J. Phys. Chem. B* **2009**, *113*, 3235–3244.
- (67) Yathindra, N.; Sundaralingam, M. *Biopolymers* **1973**, *12*, 297–314.
- (68) Although four *anti* structures can be identified on the potential energy surface for the *para* adduct (Figure 2d), only three unique structures were characterized following full optimizations. Specifically, the *anti* structure corresponding to $\chi \sim 200^\circ$ and $\theta \sim 40^\circ$ optimizes to $\chi \sim 250^\circ$ and $\theta \sim 330^\circ$.
- (69) The *para* structure corresponding to $\chi \sim 60^\circ$ and $\theta \sim 140^\circ$ and the *ortho* structures corresponding to $\chi \sim 80^\circ$, $\theta \sim 60^\circ$ and $\chi \sim 60^\circ$, $\theta \sim 310^\circ$ optimized to a C1'-*exo*-C2'-*endo* twist sugar puckering.
- (70) We note that three *anti* conformations significantly deviate from the natural β angle such that the hydroxyl group is above O4' of the sugar (*para* with $\chi \sim 220^\circ$ and $\theta \sim 210^\circ$, and *ortho* with $\chi \sim 190^\circ$ and $\theta \sim 70^\circ$ or $\chi \sim 250^\circ$ and $\theta \sim 300^\circ$). Since structures where the hydroxyl group rotated toward the nucleobase remain higher in energy than structures relevant to DNA, we do not expect these would be lower in energy if the hydroxyl group had remained in the natural orientation.
- (71) Chen, X.; Zhan, C. G. *J. Phys. Chem. B* **2008**, *112*, 16851–16859.
- (72) Poltev, V. I.; Anisimov, V. M.; Danilov, V. I.; Deriabina, A.; Gonzalez, E.; Jurkiewicz, A.; Les, A.; Polteva, N. *J. Biomol. Struct. Dyn.* **2008**, *25*, 563–571.
- (73) Shishkin, O. V.; Palamarchuk, G. V.; Gorb, L.; Leszczynski, J. *J. Phys. Chem. B* **2006**, *110*, 4413–4422.
- (74) Yathindra, N.; Sundaralingam, M. *Biopolymers* **1973**, *12*, 2075–2082.
- (75) Leulliot, N.; Ghomi, M.; Scalmani, G.; Berthier, G. *J. Phys. Chem. A* **1999**, *103*, 8716–8724.
- (76) Rubio, M.; Roca-Sanjuan, D.; Serrano-Andres, L.; Merchan, M. *J. Phys. Chem. B* **2009**, *113*, 2451–2457.
- (77) Zakjevskii, V. V.; Dolgounitcheva, O.; Zakrzewski, V. G.; Ortiz, J. V. *Int. J. Quantum Chem.* **2007**, *107*, 2266–2273.
- (78) Wiechelman, K.; Taylor, E. R. *J. Biomol. Struct. Dyn.* **1998**, *15*, 1181–1194.
- (79) Foloppe, N.; MacKerell, A. D. *Biophys. J.* **1999**, *76*, 3206–3218.
- (80) Yurenko, Y. P.; Zhurakivsky, R. O.; Ghomi, M.; Samijlenko, S. P.; Hovorun, D. M. *J. Phys. Chem. B* **2007**, *111*, 6263–6271.
- (81) For recent studies that used nucleoside models see, for example, (a) Chen, Z. Q.; Zhang, C. H.; Xue, Y. *J. Phys. Chem. B* **2009**, *113*, 10409–10420. (b) Sun, L. X.; Bu, Y. X. *THEOCHEM - J. Mol. Struct.* **2009**, *909*, 25–32. (c) Yang, Z. Z.; Qi, S. F.; Zhao, D. X.; Gong, L. D. *J. Phys. Chem. B* **2009**, *113*, 254–259. (d) Tehrani, Z. A.; Fattahi, A.; Pourjavadi, A. *Carbohydr. Res.* **2009**, *344*, 771–778. (e) Barbe, S.; Le Bret, M. *J. Comput. Chem.* **2008**, *29*, 1353–1363. (f) O'Daniel, P. I.; Jefferson, M.; Wiest, O.; Seley-Radtkie, K. L. *J. Biomol. Struct. Dyn.* **2008**, *26*, 283–292. (g) Yurenko, Y. P.; Zhurakivsky, R. O.; Ghomi, M.; Samijlenko, S. P.; Hovorun, D. M. *J. Phys. Chem. B* **2008**, *112*, 1240–1250. (h) Rios-Font, R.; Rodriguez-Santiago, L.; Bertran, J.; Sodupe, M. *J. Phys. Chem. B* **2007**, *111*, 6071–6077.
- (82) Gelbin, A.; Schneider, B.; Clowney, L.; Hsieh, S. H.; Olson, W. K.; Berman, H. M. *J. Am. Chem. Soc.* **1996**, *118*, 519–529.
- (83) Altona, C.; Sundaral, M. *J. Am. Chem. Soc.* **1973**, *95*, 2333–2344.
- (84) Chachaty, C.; Perly, B.; Forchioni, A.; Langlet, G. *Biopolymers* **1980**, *19*, 1211–1239.
- (85) Vokacova, Z.; Budesinsky, M.; Rosenberg, I.; Schneider, B.; Sponer, J.; Sychrovsky, V. *J. Phys. Chem. B* **2009**, *113*, 1182–1191.
- (86) We note that the relative energies obtained with B3LYP/6-31+G(d,p) geometries for natural dG and the *ortho* adduct are only different by 1 kJ mol^{-1} .
- (87) Gubala, V.; Betancourt, J. E.; Rivera, J. M. *Org. Lett.* **2004**, *6*, 4735–4738.
- (88) Sessler, J. L.; Jayawickramarajah, J.; Sherman, C. L.; Brodbelt, J. S. *J. Am. Chem. Soc.* **2004**, *126*, 11460–11461.